Biomass Conversion and Biorefinery (2021) 11:1407–1417
https://doi.org/10.1007/s13399-021-01593-9

ORIGINAL ARTICLE

Preparation of $ZnO/BaTiO_3$ adsorbent using *Elaeagnus Angustifolia* L. leaf extract and its evaluation for ciprofloxacin removal from aqueous solutions: an optimization study

Zeynep Ciğeroğlu[1]

Received: 9 March 2021 / Revised: 9 May 2021 / Accepted: 14 May 2021 / Published online: 22 May 2021

Abstract

Especially, most papers have reported an increase in antibiotic resistance (AR) bacterial infections during the COVID-19 pandemic. Because of the outbreak of the SARS-CoV-2, antimicrobial resistance (AMR) should be controlled and reduced. Researchers have reported that the adsorption technique is an sufficient procedure for separating drugs such as antibiotics from aqueous solutions. The prepared of $ZnO/BaTiO_3$ nanocomposite using *Elaeagnus Angustifolia* L. leaf extract was successfully obtained using green route. The synthesized nanocomposite was interacted with ciprofloxacin hydrochloride (CPF) to aim at eliminating the antibiotic from aqueous solutions. The incorporation of *Elaeagnus Angustifolia* leaf extract onto $ZnO/BaTiO_3$ proved a sustainable chemistry study. Hence, this study indicated that green nanoparticles include neither the use of hazardous chemicals nor toxic chemicals. FTIR, XRD, and SEM-EDX analyses were applied to give information about the structural properties of the green nanocomposite. Box-Behnken design (BBD) was executed by response surface methodology (RSM) to gain optimal conditions. The effect of pH, initial concentration of CPF, and nanocomposite dose on CPF-nanocomposite interaction was examined. The experimental findings of adsorption study revealed that the optimal adsorption capacity of CPF onto $ZnO/BaTiO_3$ was found as 125.29 mgg^{-1} under optimal conditions (adsorbent dose: 3.00 mg, pH value of solution: 9.88, initial concentration CPF: 49.63 mgL^{-1}).

Keywords Antibiotic resistance · Ciprofloxacin · Box-Behnken design · $ZnO/BaTiO_3$ · Adsorption · *Elaeagnus Angustifolia* L. leaf extract · Ultrasound

1 Introduction

Nowadays, antibiotic resistance (AR) is a severe topic that affects global health. Antibiotics are designed to defeat bacteria and microorganisms. These antibiotics, taken uncontrollably and unconsciously, cause the bacteria and microorganisms to gain resistance and create bacterial resistance. There are many reasons that accelerate the spread of AR. AR arises from discharging antibiotics into agricultural land, drinking water and sewage [1].

Ciprofloxacin (CPF), a second-generation fluoroquinolone, has broad-spectrum antibiotic owing to its widespread-uses in treatment for both gram-positive and gram-negative bacteria [2]. It can be used therapeutically for the lower respiratory tract, urinary tract, especially bladder infection, bone infection such as osteomyelitis, intra-abdominal infection urinary tract, skin-related infections, neutropenic patients [3].

One of the solution ways against antibiotic resistance is the process of removing antibiotics from aqueous solutions. Many techniques have been progressed to eliminate antibiotics from the aqueous phase. These are membrane technology [4], Fenton oxidation [5], photocatalytic degradation [6], electrocoagulation [7] and adsorption [8]. Among these techniques, adsorption stands out because it is the easiest, cheapest and most applicable process.

Zinc oxide (ZnO) has drawn great attention owing to its nature such as low cost, non-toxic, thermal stability [9]. Nagpal and Kakkar (2019) underlined in their review that ZnO NPs are used in wastewater treatment due to the reasons aforementioned above [10]. Nowadays, green chemistry processes in the preparation of nanoparticles are becoming more and more popular thanks to environmentally benign

✉ Zeynep Ciğeroğlu
zilbay@gmail.com; zeynep.ilbay@usak.edu.tr

[1] Department of Chemical Engineering, Engineering Faculty, Uşak University, 64300 Uşak, Turkey

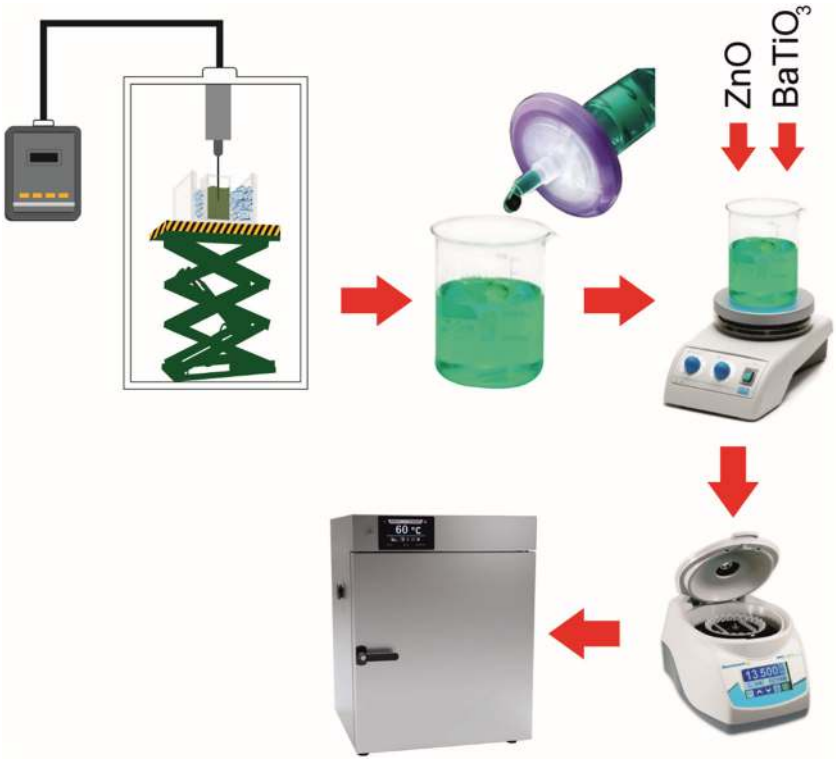

Fig. 1 The representation of the preparation of $ZnO/BaTiO_3$ using *Elaeagnus Angustifolia* leaf extract as a solvent

manufacturing. Especially, the synthesis of nanoparticles via plant extracts makes them more biocompatible [11]. Published papers related to ZnO nanoparticles exemplified the promising application of the green synthesis method [12–14]. $BaTiO_3$ is a common photocatalyst owing to the semiconductor material. When the studies in the literature were examined, it was seen that $BaTiO_3$ was scarcely used in the adsorption process. Kumari et al. (2015) prepared $BaTiO_3$-mesoporous silica nanocomposite for the extract of Cr^{6+} from water [15]. Therefore, $ZnO/BaTiO_3$ has been used for the first time in CPF adsorption.

Phytochemicals are compounds such as polyphenols, phenolic acids, and flavonoids. They contribute significantly in the reduction of metallic ions [16]. *Elaeagnus Angustifolia* known as the Russian olive has numerous phytochemicals such as flavonoids, polyphenols, phenolic acids and vitamins [17]. It is used for the treatment of ulcer, sore throat, asthma treatment, and bronchial and lung diseases [18, 19] due to its antioxidant, anticonvulsant, analgesic, and anti-inflammatory properties [17].

Response surface methodology (RSM) is widely chosen to figure out the impacts of the inputs on outcomes. RSM is a helpful statistical technique. It indicates how the responses change in the selected input range. Besides, it helps to optimize the response [20].

In this context, the ultrasound-assisted extraction method was preferred to prepare *Eleagnus Angustifolia* L. leaf extract. The prepared $ZnO/BaTiO_3$ with the help of *Eleagnus Angustifolia* L. leaf extract was used for the elimination of CPF from aqueous solutions. The secondary aim was to construct adsorption conditions containing three factors such as pH, adsorption dose, and initial concentration of CPF using RSM integrated into Box-Behnken design (BBD). Therefore, RSM was predicted to be the most suitable optimal CPF adsorption conditions, which gave the highest adsorption capacity onto $ZnO/BaTiO_3$. Both variance analysis (ANOVA) and Pareto chart were applied in order to show the impacts of inputs on the outputs. Besides, the changes of the adsorbent surface after adsorption were described using by ATR-FTIR spectroscopy. Hence, the surface morphology of the adsorbent and adsorption mechanism were illuminated.

2 Materials and methods

2.1 Materials

ZnO (99.99 %, 18 nm) and $BaTiO_3$ (99.95 %, 90 nm, cubic) were purchased from Nanografi (ODTU Teknopark, Turkey).

Table 1 Selected parameters with three levels for the adsorption of CPF onto $ZnO/BaTiO_3$

Parameters	Levels		
	-1	0	1
pH	3	7	11
Adsorbent Dose (mg)	3	6	9
Initial CPF concentration (mgL^{-1})	20	35	50

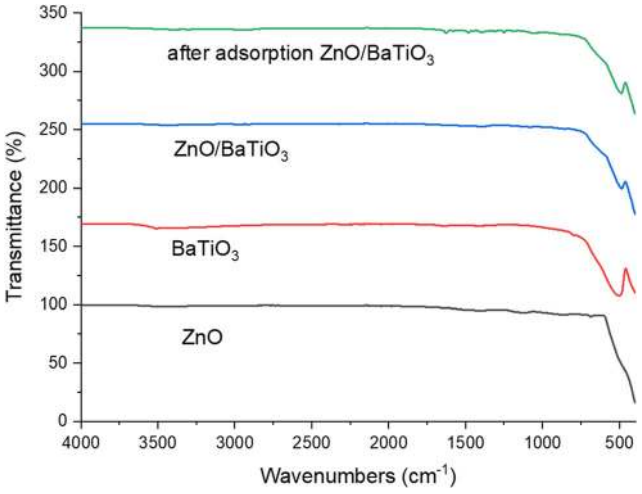

Fig. 2 FTIR spectrum of pure ZnO, pure $BaTiO_3$, $ZnO/BaTiO_3$, CPF-adsorbed ZnO /$BaTiO_3$

Elaeagnus Angustifolia L. leaves were obtained from İzmir, Turkey in 2020.

2.2 Extraction of Elaeagnus Angustifolia leaves and synthesis of $ZnO/BaTiO_3$

First, *Elaeagnus Angustifolia L.* leaves were ground by using a grinder. Then, a homogenizer (Bandelin, Sonoplus HD 2200.2) with 13 nm titanium probe was used to extract *Elaeagnus Angustifolia* L. leaf. Briefly, 30 mL of distilled water was poured into 0.75 g of grinding leaves. The sonicater was operated with a 70% amplitude (50% nominal) during 10 min. Then, the extracts were filtered using RC filter, 20 μm. 20 mL of extracts were added to the beaker and $BaTiO_3$ by taking 50 % of the weight of ZnO and ZnO were added. The solution was mixed by magnetic stirrer at a speed of 400 rpm. Absolute ethanol was used as the washing solution. After the nanoparticle was washed three times and was dried at 60 °C in a vacuum dryer until it dries. The dried material was calcinated at 550 °C during 5 h at a heating rate of 10 °C. Figure 1 represented the preparation of $ZnO/BaTiO_3$ using *Elaeagnus Angustifolia* leaf extract as a solvent.

2.3 Characterization of the prepared ZnO/BaTiO3

Spectrum Two FT-IR Spectrometer (FTIR) (Perkin Elmer) was applied to describe the functional groups of the prepared $ZnO/BaTiO_3$ nanocomposite. Scanning electron microscopy (SEM) with energy dispersive X-ray analysis (XL-30 SFEG, Philips, Eindhoven, Holland) was performed to illuminate the surface analysis of the samples. X-ray diffraction (XRD) analyses were done using (Bruker D8 Advance device) via Cu Kα radiation over a 2θ range from 2-90° with the scanning rate of 3° min^{-1}.

2.4 Adsorption experiments and statistical analysis

The design of adsorption runs were constructed using Design Expert 12 software ((Trial version 12, Stat-Ease, USA). The desired adsorbent dose was added to Erlenmayer and the specified initial antibiotic solution was poured into the Erlenmayer. Then, shaker was run at the speed of 100 rpm for two hours. Two hours later, the initial and final solution were read at 275 nm by using a UV-Vis Spectrophotometer (Pekin Elmer, Lambda 365, USA). The adsorption capacity was calculated in Eq. (1) as follows;

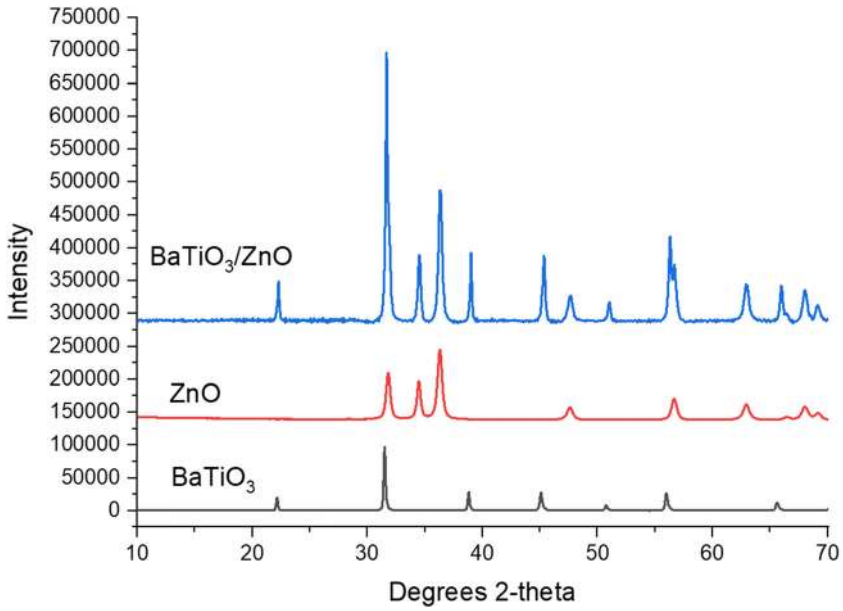

Fig. 3 XRD patterns of $BaTiO_3$, ZnO, $ZnO/BaTiO_3$

$$q_e = \frac{(C_o - C_f)xV}{m} \quad (1)$$

In Eq. (1), qe is the adsorption capacity (mg g^{-1}), C_o is the initial CPF concentration in solution (mgL^{-1}), C_f is the final concentration in 2 h later (mgL^{-1}), m is the mass of ZnO/$BaTiO_3$ (g), and V is the solution volume (L).

Response surface methodology (RSM) was preferred in order to optimize the adsorption process conditions. RSM suggested a mathematical model indicating the process conditions. By using this mathematical equation in coded factor in Eq. (2).

$$Y = \alpha_0 + \sum_{i=1}^{k} \alpha_i x_i + \sum_{i=1}^{k} \alpha_{ii} x_i^2 + \sum_{i<}^{k} \sum_{j}^{k} \alpha_{ij} x_i x_j + \varepsilon \quad (2)$$

where α_0 is the intercept, α_i is a single factor, α_{ij} is the interaction of factors and ε is a pure error.

The evaluation of the percentage effect (P %) of each variable on the adsorption capacity could be drawn Pareto chart by following Eq. (3) [21].

$$P\,(\%) = \left(\frac{\alpha_i^2}{\sum \alpha_i^2}\right) x100 \; (i \neq 0) \quad (3)$$

In Eq. (3), α_i is the coefficient of variables in Eq (2) in accordance with coded factor, P_i is the percentage of each variable, respectively.

In order to assess the impacts of the inputs (pH, CPF initial concentration and adsorbent dose) on the response (adsorption capacity), BBD design was selected. Box and Behnken devised Box-Behnken design in 1960 [22] BBD is an alternative method instead of a full factorial design serving labor efficiency with fewer essential experiments [23]. Herein, 3 factors with three levels of Box-Behnken design were applied to

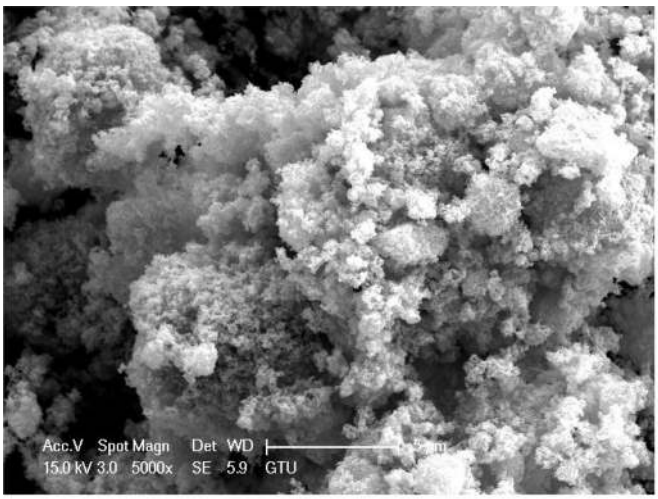

Element	Weight %	Atomic	Net Int.	Net Int. Error
O K	17.78	46.91	1199.74	0.01
ZnK	82.22	53.09	1002.72	0.01

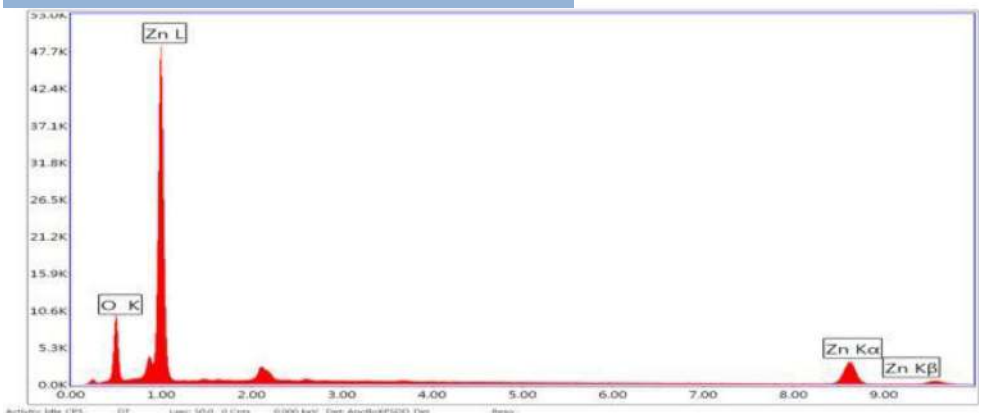

(a)

Fig. 4 SEM image and EDX spectra of **a**) ZnO, **b**) $BaTiO_3$, and **c**) ZnO/$BaTiO_3$

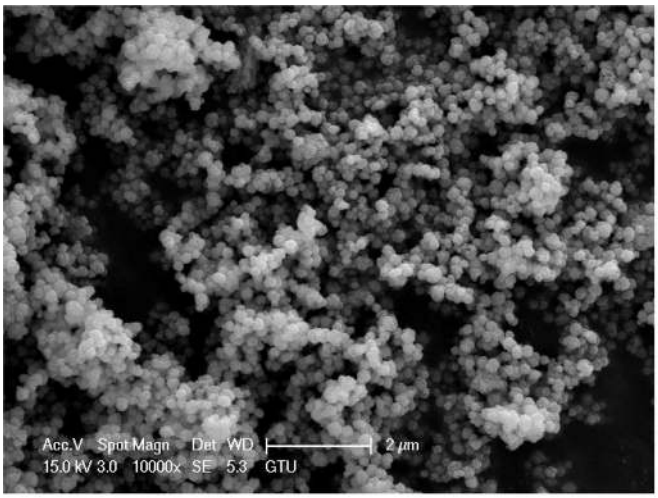

Element	Weight %	Atomic	Net Int.	Net Int. Error
O K	15.18	50.88	704.3	0.01
BaL	62.87	24.55	1537.68	0.01
TiK	21.94	24.57	1533.36	0.01

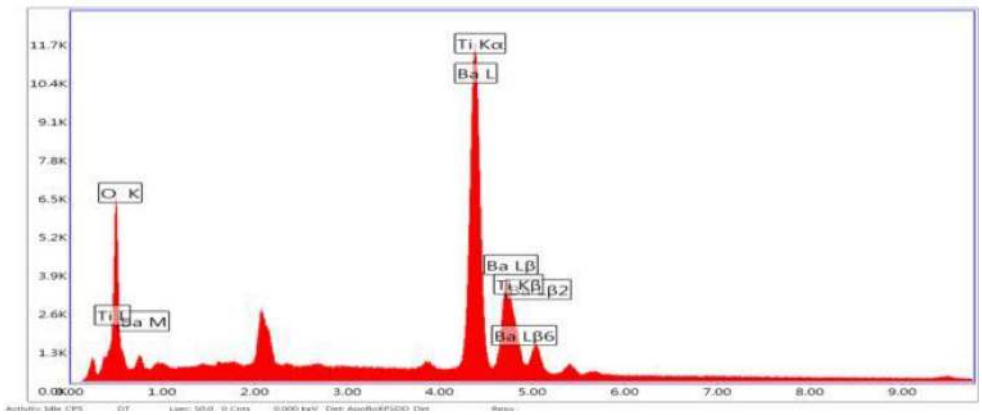

(b)

Fig. 4 (continued)

maximize the response (adsorption capacity) under the optimal conditions such as pH (A), adsorbent dose (B), and CPF initial concentration (C). Table 1 represented the coded factors.

3 Results and discussions

3.1 Characterization of ZnO, $BaTiO_3$, and ZnO/$BaTiO_3$

FTIR analysis of ZnO, $BaTiO_3$ and ZnO/$BaTiO_3$ was done using Perkin Elmer Spectrum Two IR in Fig. 2. In FTIR spectrum of $BaTiO_3$, a peak appeared at 511 cm^{-1} corresponding to a common Ti-O absorption into $BaTiO_3$ [24]. Additionally, a small peak at 3500 cm^{-1} was assigned to asymmetric and symmetric -OH bond. In ZnO FTIR's spectrum depicted that a small peak at 687 cm^{-1} was attributed to the Zn-O stretching bond [25]. FTIR spectrum of the synthesis ZnO/$BaTiO_3$ showed that the peak at around 498 cm^{-1} was the characteristic bond of Ti-O vibration [26]. The other small intensity peak at about 1400 cm^{-1} was related to the crystalline Ba-Ti-O vibration [27]. The small $(C = O)_p$ (p :pyridone) vibrations of CPF was seen at 1630 cm^{-1} in the spectrum of CPF-adsorbed ZnO/$BaTiO_3$ [28]. The other small peak emerged at 1260 cm^{-1} owing to the vibration of C–F bond of CPF [28]. This result showed that electrostatic interactions occurs between raw CPF and ZnO/$BaTiO_3$. Briefly, it was seen that there is a strong overlapping between the spectrum of CPF-adsorbed ZnO/$BaTiO_3$ and the spectrum of pure ZnO/$BaTiO_3$.

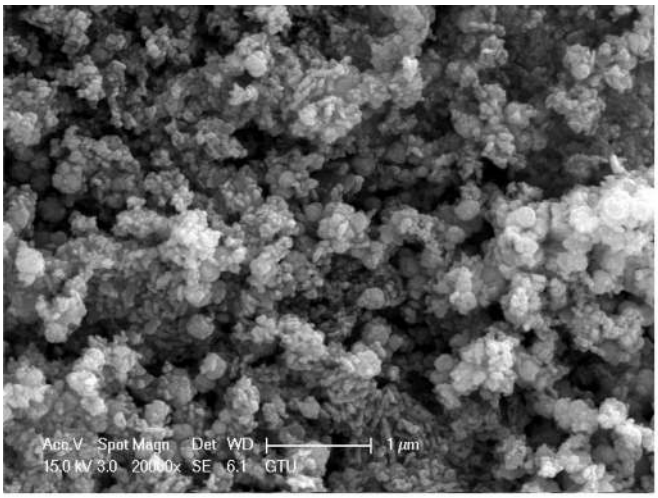

Element	Weight %	Atomic	Net Int.	Net Int. Error
O K	18.71	50.97	1117.33	0.01
BaL	19.78	6.27	519.3	0.02
TiK	7.22	6.56	519.39	0.02
ZnK	54.29	36.19	646.98	0.01

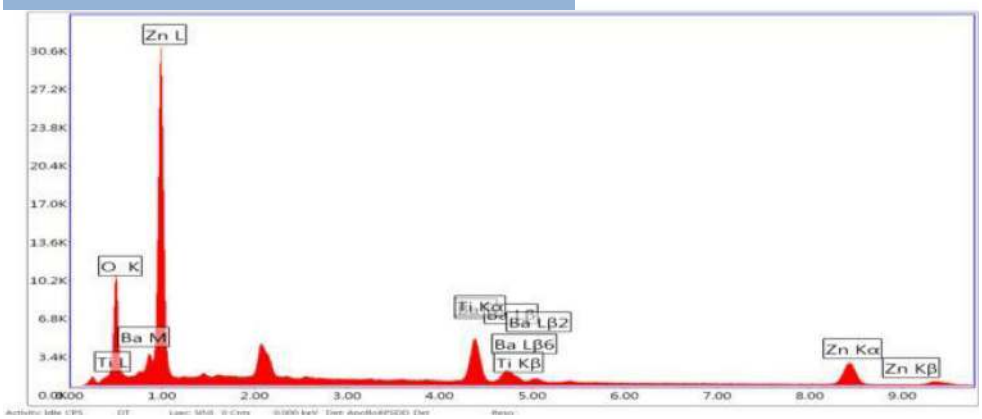

(c)

Fig. 4 (continued)

XRD pattern of $BaTiO_3$ was seen in Fig. 3. The peaks at 2θ = 22.27, 31.66, 39.02, 45.35, 51.03, 56.32, 65.98, and 69.12° were assigned to (1 0 0), (1 1 0), (1 1 1), (200), (2 1 0), (2 1 1), (2 2 0), (3 0 0) support the perovskite phase of barium titanate [29]. The peaks at 2θ = 31.67°, 34.58°, 36.02°, 47.68°, 56.68°, 62.91°, 68.02°, 69.12 indexes as (100), (002), (101), (102), (110), (103), (200), (112) of ZnO revealing the wurtzite structure of nanoparticles (Zincite, JCPDS 5-0664) [30]. The peaks related to $BaTiO_3$ and ZnO were seen in the XRD pattern of ZnO/$BaTiO_3$.

SEM image of pure $BaTiO_3$ nanoparticle showed quasi-spherical shape in Fig. 4(b). Besides, the surface of $BaTiO_3$ had less agglomerated. The agglomeration form of ZnO appeared in Fig. 4(a). In addition, the spherical shape of ZnO nanoparticles occurred. Both the spherical shape of ZnO and the quasi-spherical shape of $BaTiO_3$ belonging to the synthesized ZnO/$BaTiO_3$ were seen in Fig. 4(c). It might be claimed that a new surface occurred. A well-synthesized form of the $BaTiO_3$ and ZnO was observed from the SEM-EDX result.

3.2 Response surface design with Box-Behnken design

Seventeen runs with five replicates at center points were shown in Table 2. Through the ANOVA analysis (Table 3)

Table 2 BBD for CPF adsorption onto $ZnO/BaTiO_3$

No	pH	Adsorbent dose (mg)	CPF concentration ($mgL^{-}1$)	Adsorption capacity ($qe:mgg^{-}1$)
1	7	6	35	47.84
2	7	6	35	45.34
3	7	6	35	46.52
4	4	6	50	22.1
5	7	9	20	26.23
6	10	3	35	109.21
7	10	9	35	54.54
8	4	3	35	60.02
9	4	9	35	35.38
10	7	3	50	92.06
11	7	6	35	50.81
12	10	6	20	35.24
13	4	6	20	5.18
14	7	6	35	48.62
15	7	9	50	52.84
16	7	3	20	54.09
17	10	6	50	82.27

with the F and p-value indicates which parameter is more crucial than the others. The most effective variable was seen as pH (*F*-value: 229.19 and *p*-value<0.0001). It can be sorted by other effective parameters as follows; dose of nanoparticle (B), CPF initial concentration (C), and the squared dose of nanoparticle (B^2). In addition to variance analysis, Pareto chart serves as a better understand which parameter is more significant than the others. Hence, Pareto chart implies the percentage values of factors that are statistically crucial.

Table 3 Variance analysis for CPF adsorption onto $ZnO/BaTiO_3$

Source	Sum of squares	df	Mean square	*F*-value	*p*-value	
Model	10171.25	9	1130.14	82.40	< 0.0001	significant
A-pH	3143.45	1	3143.45	229.19	< 0.0001	
B-adsorbent dose	2678.75	1	2678.75	195.31	< 0.0001	
C-CPF initial concentration	2065.00	1	2065.00	150.56	< 0.0001	
AB	225.45	1	225.45	16.44	0.0048	
AC	226.65	1	226.65	16.53	0.0048	
BC	32.26	1	32.26	2.35	0.1690	
A^2	10.42	1	10.42	0.7596	0.4123	
B^2	1446.43	1	1446.43	105.46	< 0.0001	
C^2	425.74	1	425.74	31.04	0.0008	
Residual	96.01	7	13.72			
Lack of Fit	78.59	3	26.20	6.01	0.0579	not significant
Pure Error	17.42	4	4.36			
Cor Total	10267.26	16				
Std. Dev.	3.70		R^2		0.9906	
Mean	51.08		Adjusted R^2		0.9786	
C.V. %	7.25		Predicted R^2		0.8749	
			Adeq Precision		36.1144	

The mathematical equation in terms of coded factor was obtained as the following Eq. (4).

$$qe = 47.82 + 19.82A - 18.3B + 16.07C - 7.51AB + 7.53AC - 2.84BC - 1.57A^2 + 18.53B^2 - 10.06C^2 \quad (4)$$

The Pareto graph of the independent factors was drawn with the help of Eqs. (3) and (4). Looking at the Pareto chart in Fig. 5, the most influential factor was seen as A: (25.28%). Then, the other impacted parameters could be listed as the squared adsorbent dose (B^2: 22.09%), adsorbent dose (B: 21.55), CPF initial concentration (C: 16.62%).

The suggested model is well-fitted to the adsorption data because the lack of fit (LOF) is not significant (*p*-value=0.0579) and this value is also related to pure error containing replicates at center points. The higher R^2 value (0.9906) demonstrated a higher regression between the proposed data and empirical results. The obtained higher R^2- adj (0.9786) showed a reliable correlation. The difference between R^2-adj and R^2-pred was calculated as 0.1037. This value implied that the suggested model estimated the outcomes properly.

Generating 3-D surface graphs allow researchers to interpret the relationships between dependent and independent parameters more easily. The desired maximum adsorption capacity was found as 125.29 mgg^{-1} under optimal conditions such as the adsorbent dose: 3.00 mg, pH value of the solution: 9.88, initial concentration CPF:49.63 mgL^{-1}.

Adsorption studies have revealed that pH of the solution plays an effective factor on adsorption mechanism as a result of the surface charge of the adsorbent is varied with pH [31]. While the pH value of the solution was increasing, the adsorption capacity of CPF onto $ZnO/BaTiO_3$ was increased. The adsorption capacity was obtained from 57 to 126 mgg^{-1} from pH 4 to pH 10 (Fig. 6 (a)–(b)). Similar result was recorded by Sun et al. (2016) [32]. In order to explain the higher adsorption

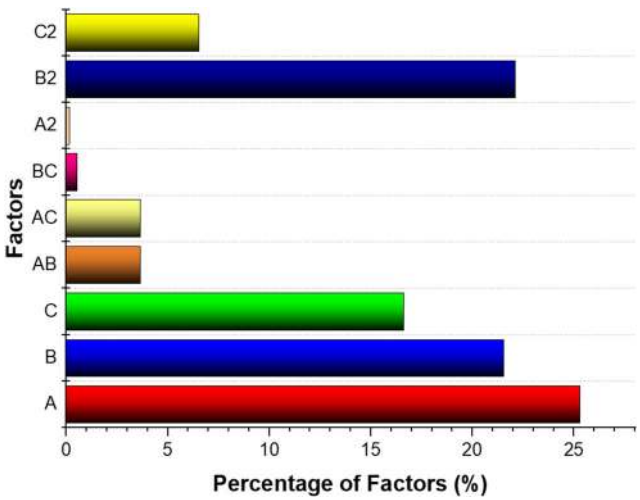

Fig. 5 Pareto graph for the adsorption capacity of CPF onto $ZnO/BaTiO_3$

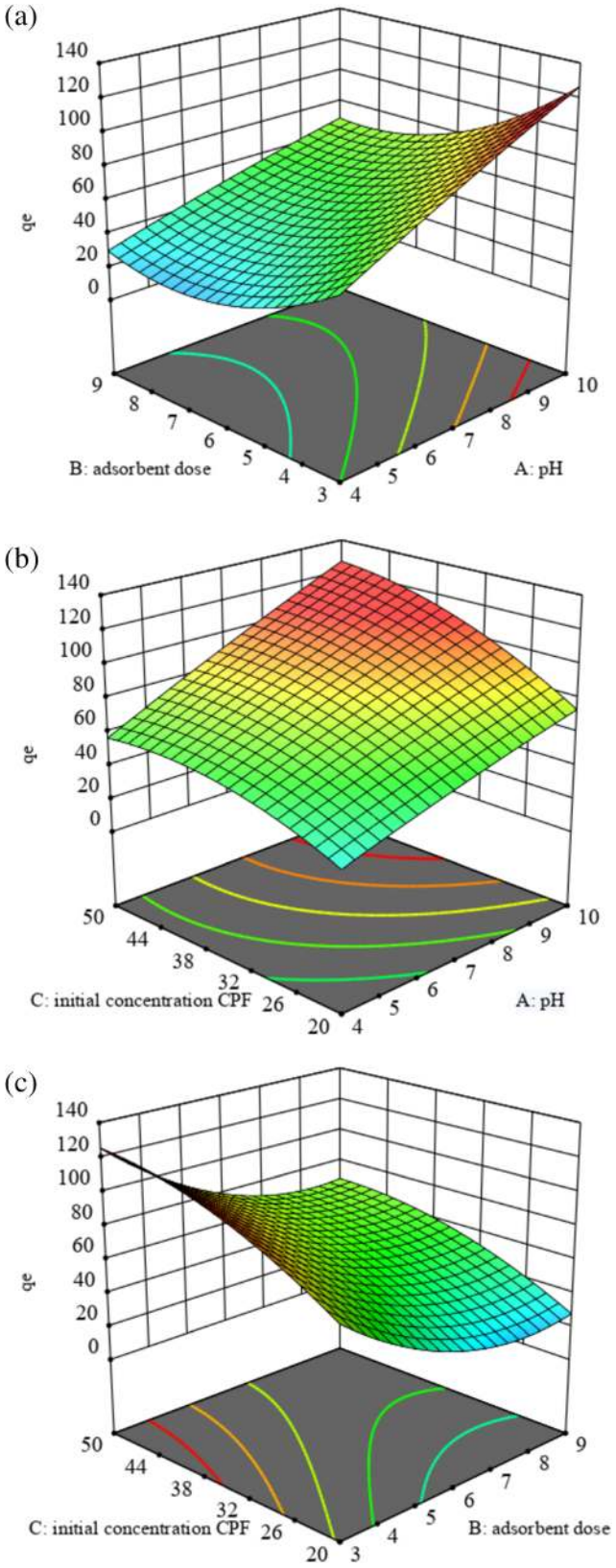

Fig. 6 The binary interaction of inputs on qe a) pH-adsorbent dose, b) pH-initial CPF concentration, c) adsorbent dose-initial CPF concentration under optimal conditions (adsorbent dose: 3.00 mg, pH value of solution: 9.88, initial concentration CPF: 49.63 $mgL^{-}1$)

Table 4 The maximum adsorption capacity for ZnO/$BaTiO_3$ and green adsorbents recorded in the literature for CPF adsorption

Adsorbent	qmax (mgg^{-1})	Reference
amine- functionalized bio graphene	172.6	[41]
Fe_2O_3–Dy_2O_3 (FD)	125	[42]
c-Fe_2O_3–Dy_2O_3 (c-FD)	328	
(C: Syzygium aromaticum (Clove)) BC-2-650	449.40	[43]
(magnetic biochar of camphor leaf , $ZnCl_2$/biochar mass ratio of 2, Calcination: 650 °C) ZnO/$BaTiO_3$	125.29 mgg-1	This Study

capacity in basic pH, it is necessary to know the pKa values of the CPF antibiotic. CPF has two pKa values, which are pKa_1: 5.90 and pKa_2: 8.89 owing to the presence of the carboxyl group and amine groups in piperazine ring, respectively [33]. Thus, three different forms such as cationic CPF^+ (pK_{a1}), zwitterionic CPF± (between the pK_{a1} and pK_{a2}) and anionic CPF^- (pK_{a2}) occurred [34]. Thus, the electrostatic interaction between the anionic adsorbate and cationic charged adsorbent occurred in basic pH.

While varying ZnO/$BaTiO_3$ dose value from 3 mg to 9 mg, the adsorption capacity was decreased (Fig. 6 (a)–(c)). Obviously, the higher adsorption capacity is obtained by using the lesser adsorbent dose. Besides, increasing the amount of adsorbent brings about both the aggregation of green adsorbent and the improvement of electrostatic repulsive force between green nanoparticles [35]. Thus, CPF molecules are difficult to interact with the adsorbent. Similar data were recorded by Yu et al. (2018) [36] and Li et al. (2017) [37].

Numerous CPF concentrations (20-50 mgL^{-1}) were prepared to assess the impact of initial CPF concentration on the adsorption process. The higher adsorption capacity was gained, when the initial CPF concentration was 50 mgL^{-1}(Fig. 6 (b)–(c)). This situation is clearly explained that, a high initial concentration of CPF results in higher concentration gradient owing to the driving force [38]. Thus, CPF molecules were adsorbed faster to the surface of ZnO/$BaTiO_3$. However, the rapid increment of adsorption capacity was gradually decreased after the certain CPF initial concentration, because of the saturation of adsorbent's active sites by higher concentration of CPF [39]. The repulsion between the CPF and adsorbent happens by the virtue of the occupation of CPF onto available sites of adsorbent [40].

The high qe of adsorbent is a crucial factor for the utilization of the adsorbent from an economic point of view. ZnO/$BaTiO_3$ exhibited a good adsorbent for the adsorption of CPF. The measured qmax for ZnO/$BaTiO_3$ and green adsorbents recorded in the literature were summarized in Table 4. Hence, ZnO/$BaTiO_3$ is a promising adsorbent and can be used for the removal of antibiotics.

4 Conclusion

To sum up, this work examined the valorization of *Elaeagnus Angustifolia* L. leaf as a high potential reducing agent to prepare ZnO/$BaTiO_3$ nanoparticles. The leaves, which are also described as biowaste, were extracted by selecting the innovative extraction method. Thus, the ultrasound-assisted extraction method offers less extraction time, lower energy consumption, and lower solvent consumption. In this context, the extraction method chosen is also an environmentally friendly method. Box-Behnken design (BBD) gives a better outcome for optimization by reducing the number of experiments. The effects of pH, initial concentration of CPF, nanocomposite dose on CPF-nanocomposite interaction were examined as independent factors. The maximum adsorption capacity of CPF onto ZnO/$BaTiO_3$ was found as 125.29 mgg^{-1} under optimal conditions (adsorbent dose:3.00 mg, pH value of solution: 9.88, initial concentration CPF:49.63 mgL^{-1}). Pareto graph was indicated that the most influential factor was pH (25.28%).

Acknowledgements The author would like to thank Bilim Pharmaceuticals for support Ciprofloxacin HCl.

References

1. Pei R, Kim S-C, Carlson KH, Pruden A (2006) Effect of River Landscape on the sediment concentrations of antibiotics and corresponding antibiotic resistance genes (ARG). Water Res 40:2427–2435. https://doi.org/10.1016/j.watres.2006.04.017
2. King DE, Malone R, Lilley SH (2000 May 1) New classification and update on the quinolone antibiotics. Am Fam Physician 61(9): 2741–2748
3. Lew MA, Kehoe K, Ritz J et al (1991) Prophylaxis of bacterial infections with ciprofloxacin in patients undergoing bone marrow transplantation. Transplantation 51:630–636. https://doi.org/10.1097/00007890-199103000-00017
4. Riquelme Breazeal MV, Novak JT, Vikesland PJ, Pruden A (2013) Effect of wastewater colloids on membrane removal of antibiotic resistance genes. Water Res 47:130–140. https://doi.org/10.1016/j.watres.2012.09.044

5. Elmolla ES, Chaudhuri M, Eltoukhy MM (2010) The use of artificial neural network (ANN) for modeling of COD removal from antibiotic aqueous solution by the Fenton process. J Hazard Mater 179:127–134. https://doi.org/10.1016/j.jhazmat.2010.02.068
6. Elmolla ES, Chaudhuri M (2010) Photocatalytic degradation of amoxicillin, ampicillin and cloxacillin antibiotics in aqueous solution using UV/TiO2 and UV/H2O2/TiO2 photocatalysis. Desalination 252:46–52. https://doi.org/10.1016/j.desal.2009.11.003
7. Yoosefian M, Ahmadzadeh S, Aghasi M, Dolatabadi M (2017) Optimization of electrocoagulation process for efficient removal of ciprofloxacin antibiotic using iron electrode; kinetic and isotherm studies of adsorption. J Mol Liq 225:544–553. https://doi.org/10.1016/j.molliq.2016.11.093
8. Danalıoğlu ST, Bayazit ŞS, Kerkez Kuyumcu Ö, Salam MA (2017) Efficient removal of antibiotics by a novel magnetic adsorbent: Magnetic activated carbon/chitosan (MACC) nanocomposite. J Mol Liq 240:589–596. https://doi.org/10.1016/j.molliq.2017.05.131
9. Ul Haq B, AlFaify S, Alshahrani T, Ahmed R, Mahmood Q, Hoat DM, Tahir SA (2021) Investigations of thermoelectric properties of ZnO monolayers from the first-principles approach. Phys E Low-dimensional Syst Nanostructures 126:114444. https://doi.org/10.1016/j.physe.2020.114444
10. Nagpal M, Kakkar R (2019) Use of metal oxides for the adsorptive removal of toxic organic pollutants. Sep Purif Technol 211:522–539. https://doi.org/10.1016/j.seppur.2018.10.016
11. Rajan R, Chandran K, Harper SL, Yun SI, Kalaichelvan PT (2015) Plant extract synthesized silver nanoparticles: An ongoing source of novel biocompatible materials. Ind Crop Prod 70:356–373. https://doi.org/10.1016/j.indcrop.2015.03.015
12. Palai P, Muduli S, Priyadarshini B, Sahoo TR (2021) A facile green synthesis of ZnO nanoparticles and its adsorptive removal of Congo red dye from aqueous solution. Mater Today Proc 38:2445–2451. https://doi.org/10.1016/j.matpr.2020.07.387
13. Ramesh M, Anbuvannan M, Viruthagiri G (2015) Green synthesis of ZnO nanoparticles using Solanum nigrum leaf extract and their antibacterial activity. Spectrochim Acta Part A Mol Biomol Spectrosc 136:864–870. https://doi.org/10.1016/j.saa.2014.09.105
14. Vijayakumar S, Vaseeharan B, Malaikozhundan B, Shobiya M (2016) Laurus nobilis leaf extract mediated green synthesis of ZnO nanoparticles: Characterization and biomedical applications. Biomed Pharmacother 84:1213–1222. https://doi.org/10.1016/j.biopha.2016.10.038
15. Kumari V, Sasidharan M, Bhaumik A (2015) Mesoporous BaTiO 3@ SBA-15 derived via solid state reaction and its excellent adsorption efficiency for the removal of hexavalent chromium from water. Dalton Trans 44:1924–1932
16. Makarov VV, Love AJ, Sinitsyna OV, Makarova SS, Yaminsky IV, Taliansky ME, Kalinina NO (2014) "Green" nanotechnologies: synthesis of metal nanoparticles using plants. Acta Naturae (англоязычная версия) 6(1):20
17. Hamidpour R, Hamidpour S, Hamidpour M, Shahlari M, Sohraby M, Shahlari N, Hamidpour R (2016) Russian olive (Elaeagnus angustifolia L.): From a variety of traditional medicinal applications to its novel roles as active antioxidant, anti-inflammatory, anti-mutagenic and analgesic agent. J Tradit Complement Med 7(1):24–29. https://doi.org/10.1016/j.jtcme.2015.09.004
18. Natanzi MM, Pasalar P, Kamalinejad M, et al (1970) Effect of Aqueous Extract of Elaeagnus angustifolia Fruit on Experimental Cutaneous Wound Healing in Rats. Acta Med Iran 50
19. Mahboubi M (2018) Elaeagnus angustifolia and its therapeutic applications in osteoarthritis. Ind Crop Prod 121:36–45. https://doi.org/10.1016/j.indcrop.2018.04.051
20. Ye G, Ma L, Li L, Liu J, Yuan S, Huang G (2020) Application of Box–Behnken design and response surface methodology for modeling and optimization of batch flotation of coal. Int J Coal Prep Util 40:131–145. https://doi.org/10.1080/19392699.2017.1350657
21. Khuri AI, Cornell JA (2018). Response surfaces: designs and analyses. Routledge.
22. Box GEP, Behnken DW (1960) Some New Three Level Designs for the Study of Quantitative Variables. Technometrics. 2:455–475. https://doi.org/10.1080/00401706.1960.10489912
23. Simsek S, Uslu S (2020) Investigation of the effects of biodiesel/2-ethylhexyl nitrate (EHN) fuel blends on diesel engine performance and emissions by response surface methodology (RSM). Fuel 275:118005. https://doi.org/10.1016/j.fuel.2020.118005
24. de Gomes MA, Magalhães LG, Paschoal AR et al (2018) An Eco-Friendly Method of BaTiO3 Nanoparticle Synthesis Using Coconut Water. J Nanomater 2018:5167182–5167187. https://doi.org/10.1155/2018/5167182
25. Lamba R, Umar A, Mehta SK, Kansal SK (2015) Sb2O3–ZnO nanospindles: A potential material for photocatalytic and sensing applications. Ceram Int 41:5429–5438. https://doi.org/10.1016/j.ceramint.2014.12.109
26. Slimani Y, Selmi A, Hannachi E, Almessiere MA, Baykal A, Ercan I (2019) Impact of ZnO addition on structural, morphological, optical, dielectric and electrical performances of BaTiO3 ceramics. J Mater Sci Mater Electron 30:9520–9530. https://doi.org/10.1007/s10854-019-01284-2
27. Kappadan S, Gebreab TW, Thomas S, Kalarikkal N (2016) Tetragonal BaTiO3 nanoparticles: An efficient photocatalyst for the degradation of organic pollutants. Mater Sci Semicond Process 51:42–47. https://doi.org/10.1016/j.mssp.2016.04.019
28. Sasikumar S (2013) Effect of particle size of calcium phosphate based bioceramic drug delivery carrier on the release kinetics of ciprofloxacin hydrochloride: an in vitro study. Front Mater Sci 7:261–268. https://doi.org/10.1007/s11706-013-0216-6
29. Singh DK, Mondal K, Manam J (2017). Improved photoluminescence, thermal stability and temperature sensing performances of K^+ incorporated perovskite $BaTiO_3$: Eu^{3+} red emitting phosphors. Ceram Int 43:13602–13611. https://doi.org/10.1016/j.ceramint.2017.07.069
30. Akhtar MJ, Ahamed M, Kumar S et al (2012) Zinc oxide nanoparticles selectively induce apoptosis in human cancer cells through reactive oxygen species. Int J Nanomedicine 7:845–857. https://doi.org/10.2147/IJN.S29129
31. Babel S, Kurniawan TA (2004) Cr(VI) removal from synthetic wastewater using coconut shell charcoal and commercial activated carbon modified with oxidizing agents and/or chitosan. Chemosphere 54:951–967. https://doi.org/10.1016/j.chemosphere.2003.10.001
32. Sun Y, Li H, Li G, Gao B, Yue Q, Li X (2016) Characterization and ciprofloxacin adsorption properties of activated carbons prepared from biomass wastes by H3PO4 activation. Bioresour Technol 217:239–244. https://doi.org/10.1016/j.biortech.2016.03.047
33. Roca Jalil ME, Baschini M, Sapag K (2015) Influence of pH and antibiotic solubility on the removal of ciprofloxacin from aqueous media using montmorillonite. Appl Clay Sci 114:69–76. https://doi.org/10.1016/j.clay.2015.05.010
34. Gu C, Karthikeyan KG (2005) Sorption of the Antimicrobial Ciprofloxacin To Aluminum and Iron Hydrous Oxides. Environ Sci Technol 39:9166–9173. https://doi.org/10.1021/es051109f
35. Mesbah M, Hamedshahraki S, Ahmadi S, Sharifi M, Igwegbe CA (2020) Hydrothermal synthesis of LaFeO3 nanoparticles adsorbent: Characterization and application of error functions for adsorption of fluoride. MethodsX 7:100786. https://doi.org/10.1016/j.mex.2020.100786
36. Yu F, Chen D, Ma J (2018) Adsorptive removal of ciprofloxacin by ethylene diaminetetraacetic acid/β-cyclodextrin composite from

aqueous solution. New J Chem 42:2216–2223. https://doi.org/10.1039/C7NJ03770H
37. Li S, Zhang X, Huang Y (2017) Zeolitic imidazolate framework-8 derived nanoporous carbon as an effective and recyclable adsorbent for removal of ciprofloxacin antibiotics from water. J Hazard Mater 321:711–719. https://doi.org/10.1016/j.jhazmat.2016.09.065
38. Ciğeroğlu Z, Küçükyıldız G, Haşimoğlu A, Taktak F, Açıksöz N (2020) Fast and effective methylene blue adsorption onto graphene oxide/amberlite nanocomposite: Evaluation and comparison of optimization techniques. Korean J Chem Eng 37:1975–1984. https://doi.org/10.1007/s11814-020-0600-8
39. Igwegbe CA, Mohmmadi L, Ahmadi S, Rahdar A, Khadkhodaiy D, Dehghani R, Rahdar S (2019) Modeling of adsorption of Methylene Blue dye on Ho-CaWO4 nanoparticles using Response Surface Methodology (RSM) and Artificial Neural Network (ANN) techniques. MethodsX 6:1779–1797. https://doi.org/10.1016/j.mex.2019.07.016
40. Rahdar S, Rahdar A, Zafar MN, Shafqat SS, Ahmadi S (2019) Synthesis and characterization of MgO supported Fe–Co–Mn nanoparticles with exceptionally high adsorption capacity for Rhodamine B dye. J Mater Res Technol 8:3800–3810. https://doi.org/10.1016/j.jmrt.2019.06.04
41. Ghadiri SK, Alidadi H, Tavakkoli Nezhad N, Javid A, Roudbari A, Talebi SS, Mohammadi AA, Shams M, Rezania S (2020) Valorization of biomass into amine-functionalized bio graphene for efficient ciprofloxacin adsorption in water-modeling and optimization study. PLoS One 15(4):e0231045
42. Jain A, Sharma A, Kapur A et al (2021) Hematite dysprosium oxide nanocomposites biosynthesized via greener route for ciprofloxacin removal and antimicrobial activity. J Nanostructure Chem. https://doi.org/10.1007/s40097-020-00379-1
43. Hu Y, Zhu Y, Zhang Y, Lin T, Zeng G, Zhang S, Wang Y, He W, Zhang M, Long H (2019) An efficient adsorbent: Simultaneous activated and magnetic ZnO doped biochar derived from camphor leaves for ciprofloxacin adsorption. Bioresour Technol 288:121511. https://doi.org/10.1016/j.biortech.2019.121511